Mutual diffusion in binary Ar-Kr mixtures and empirical diffusion models

Yanhua Zhou and Gregory H. Miller
Department of Geophysical Sciences, University of Chicago, 5734 South Ellis Avenue, Chicago, Illinois 60637
(Received 13 March 1995; revised manuscript received 28 June 1995)

Molecular dynamics simulations of four binary Ar-Kr mixtures are used to compute self- and mutual-diffusion coefficients. Results using mean squared displacements and using velocity correlation functions are presented. The diffusivity coefficients are also presented in the time and frequency domains where a comparatively low frequency structure is evident in some simulations. The computed diffusivities are dependent on the maximum time over which the velocity correlation functions are integrated and the time at which the Einstein relationships are evaluated. This dependence explains in part the small systematic differences between our results (20–80 ps) and earlier molecular dynamics results (<4 ps) in the system Ar-Kr. We compare the computed mutual diffusion coefficients to two empirical models, Darken's model and the common force model. Darken's model is consistent with our results over the entire frequency range we resolve. At frequencies lower than about 5 ps^{-1} Darken's model and the common force model converge and we cannot discriminate between them. At higher frequencies the common force model prediction is significantly different from the computed mutual diffusion coefficient. Assumptions regarding the contribution of cross correlations that are implicit in the empirical models are discussed and tested against our simulation results. The net contribution of velocity cross correlations is found to be negligible, as is often assumed in deriving Darken's model, but the individual cross-correlation terms are substantial and negative—a finding contrary to common assumptions.

PACS number(s): 05.60.+w, 05.70.Ln, 82.20.Wt, 82.20.Mj

I. INTRODUCTION

Mutual diffusion, also called chemical diffusion or interdiffusion, describes the transport of mass driven by gradients in chemical potential. In geological systems multicomponent chemical diffusion is related to such processes as oscillatory zoning in crystals, double diffusive convection in magmas, partial melting of the mantle, and isotopic and chemical exchange in silicate melts [1–4]. The complexity of these phenomena is in striking contrast to the apparent simplicity of Fick's law.

Strictly speaking, under isothermal and isobaric conditions chemical diffusion in an n-component system can be described by an $(n-1)\times(n-1)$ composition- and reference-frame-dependent diffusivity matrix [5]. The chemical complexity of natural magma compositions makes it impractical to specify this full diffusivity matrix for every system of geological interest. Instead, empirical diffusion models are often employed. A number of such models have been proposed in experimental studies of diffusion in glasses, metal and silicate melts, and aqueous solutions [6–10]. In this paper we will consider two particular models that predict different relationships between the mutual-diffusion coefficients, the n self-diffusivities, and other thermodynamic quantities such as partial molar volumes.

One of the diffusion models we consider is called Darken's model [7] or the Hartley-Crank equation [11] in binary systems, and Cooper's model in multicomponent systems [8]. This model gives the diffusion flux of a species, say i, as the sum of two terms. The first term describes the diffusion of i in response to gradients in its own chemical potential. The phenomenological coefficient in this first term is taken to be the self-diffusivity of component i. The second term describes the advection of i with a velocity called the relaxation velocity, and which is common to all chemical species. The relaxation velocity is determined by requiring that there be no net volume flux [12]. The chemical diffusivities are given in terms of the self-diffusivities by expressing the relaxation velocity in terms of the n component fluxes.

In molten silicates a model based on a common relaxation force describes experimental results better than the Darken common relaxation velocity model [10]. In its simplest form this "common force" model is mathematically equivalent to Lasaga's [9] model for cation diffusion in an anion-fixed reference frame. There the cations, assumed of equal charge, are subject to the same electrostatic repulsion force. This model has found application to both electrolyte and nonelectrolyte solutions [13]. In uncharged systems the value of the common force is again determined by a constraint of zero net volume flux. The chemical diffusivities may be expressed in terms of the self-diffusivities by expressing the common force in terms of the component fluxes.

In this study we test these empirical models in binary argon (Ar)–krypton (Kr) mixtures using molecular dynamics simulations. Molecular dynamics is well suited to the study of transport properties of liquids since it allows the diffusive motions of each particle to be "observed" on atomic scales of length and time (e.g., [14,15]). The chemical and self-diffusion coefficients of a binary system may be computed simultaneously in a single simulation. We determine these coefficients by two methods and test them for consistency with the empirical diffusion models.

In Ar-Kr we find good agreement with Darken's model, which is what one might anticipate since the derivation of Darken's model often appeals to "ideality" [11,16]. However, "ideality" is not evident in the velocity cross correlations seen in the simulation. That is, Darken's model works despite the failure of a common model assumption. Thus there is a need to develop a more general understanding of the relationship between chemical properties and the heuristic diffusion models most appropriate to them.

In the statistical theory of liquids phenomenological diffusion coefficients are expressed as the time integrals of correlations of functions of microscopic particle velocities, i.e., the Green-Kubo formulas [17]. Chemical and self-diffusivities are related to the velocity correlation functions of collective motions of the system and of single-particle motions, respectively. Darken's model and the common force model each require different relationships amongst the cross-correlation terms. For Darken's model to apply the sum of the contributions of the cross correlations must be zero. This is consistent with, but does not require, ideality. The cumulative effect of cross correlation is negative in the common force model, and so in binary systems the common force interdiffusion coefficient is less than the Darken model value.

The Green-Kubo formulas are evaluated by integrating the correlation functions over time from zero to infinity. In practice the upper limit of integration is rarely greater than a few picoseconds [18–20]. We examine the effect of this practice by computing the Fourier spectra of the velocity correlation functions, and thereby defining frequency-dependent diffusivities. The zero-frequency limit of the frequency-dependent diffusivity corresponds to the usual macroscopic diffusivity, but this term cannot be uniquely determined in a picosecond time scale experiment if low frequency modes of the system are present. The effect of truncating the Green-Kubo integrals may be qualitatively assessed by examining the frequency structure of the frequency-dependent diffusivities. If the slope of diffusivity with frequency is non-negligible at the lowest resolved frequencies then truncating the upper limit of integration is likely to have a measurable effect. When no frequency dependence is seen at low frequencies it is possible, though not certain, that the truncation is inconsequential.

Frequency- or time-dependent diffusivity at short times has been observed experimentally [21–24] and in numerical simulations of colloidal particles [25,26].

We also calculate diffusion coefficients using the Einstein relations [16]. This method is based on the time dependence of the mean squared displacement of specified modes of the system. Self-diffusivities are determined from the displacement of individual particles; mutual diffusivities are found from the displacement of a collective particle mode. Einstein diffusivities are formally equivalent to Green-Kubo diffusivities when evaluated at infinite time. The relationship between these models when truncated at a finite time is described.

In Sec. II A we introduce the empirical diffusion models starting from the phenomenological equations of nonequilibrium thermodynamics. The relationship between these macroscopic phenomenological coefficients and the microscopic particle trajectories "seen" in molecular dynamics simulations is presented in Sec. II B. In Sec. III some details regarding our numerical simulations are described, and in Sec. IV the simulation results for the self-diffusivity of Ar and of Kr and for their mutual diffusion are presented. These results are discussed in the context of the empirical models in Sec. V. Finally, we present our conclusions in Sec. VI.

II. EMPIRICAL DIFFUSION MODELS

In this section we develop a complete phenomenological model for multicomponent diffusion. Phenomenological developments of Cooper's model and the common force model are also presented. Next, we describe the relationship between the phenomenological diffusivity coefficients and microscopic statistical properties of the system. We show that reduction of the binary mutual-diffusion coefficient to the empirical model equations requires specific relationships amongst the velocity cross-correlation functions. This provides the theoretical background necessary to "measure" diffusion coefficients in a simulation, and to test the validity of the assumptions implicit in the empirical models.

A. The phenomenological equations

Consider an n-component system under conditions of constant pressure P and temperature T. According to the theory of nonequilibrium thermodynamics [5], the entropy production per unit volume and the unit time, σ, can be written as a sum of n products of diffusion fluxes $\mathbf{J}_i$ and associated thermodynamic "forces" $\nabla\mu_i/T$:

$$\sigma = -\sum_{i=1}^{n} \mathbf{J}_i \cdot \left[\frac{\nabla \mu_i}{T} \right] . \tag{1}$$

Here, μ_i is the molar chemical potential of species i. The phenomenological equations may be written quite generally as

$$\mathbf{J}_i = -\sum_{k=1}^{n} l_{ik} \frac{\nabla \mu_k}{T} \quad (i=1,2,\ldots,n) , \tag{2}$$

where l_{ik} is a set of n^2 phenomenological coefficients. At thermodynamic equilibrium the average values of σ, $\mathbf{J}_i$, and $\nabla\mu_i$ vanish.

In laboratory experiments the diffusion fluxes are usually defined relative to a volumetric reference velocity $\mathbf{u}^V$,

$$\mathbf{J}_i^V = \rho_i(\mathbf{u}_i - \mathbf{u}^V) \quad (i=1,2,\ldots,n) , \tag{3a}$$

with

$$\mathbf{u}^V = \sum_{i=1}^{n} \bar{V}_i \rho_i \mathbf{u}_i , \tag{3b}$$

where $\bar{V}_i$ is the partial molar volume of component i, $\mathbf{u}_i$ its velocity, and $\mathbf{J}_i^V$ its molar flux. ρ_i is the mole density of species i, and the total molar density is given by

$\rho=\sum_{i=1}^{n}\rho_i$. The condition $\mathbf{u}^V=\mathbf{0}$, defining the volume-fixed reference frame, is commonly assumed.

The continuity equation

$$\sum_{i=1}^{n}\bar{V}_i\mathbf{J}_i^V=0 \tag{4}$$

places a constraint on the n diffusion fluxes, and we may use this constraint to eliminate one flux, say $\mathbf{J}_n^V$, from (1). Then the entropy production may be described by the remaining $n-1$ fluxes and new associated forces:

$$\sigma=-\sum_{i=1}^{n-1}\mathbf{J}_i^V\cdot\left[\frac{\nabla\mu_i}{T}-\frac{\bar{V}_i}{\bar{V}_n}\frac{\nabla\mu_n}{T}\right] . \tag{5}$$

The $n-1$ phenomenological equations implied by (5) are

$$\mathbf{J}_i^V=-\sum_{k=1}^{n-1}L_{ik}\left[\frac{\nabla\mu_k}{T}-\frac{\bar{V}_k}{\bar{V}_n}\frac{\nabla\mu_n}{T}\right] \quad (i=1,2,\ldots,n-1) , \tag{6}$$

and the nth flux $\mathbf{J}_n^V$ is given by (4). The new phenomenological coefficients L_{ik} can be related to the l_{ik} by equating individual terms in (2) with corresponding ones in (6).

The Gibbs-Duhem equations provide a constraint on the thermodynamic forces:

$$\sum_{i=1}^{n}\rho_i\nabla\mu_i=0 . \tag{7}$$

Using (7) to eliminate $\nabla\mu_n$ from (5) we obtain

$$\sigma=-\sum_{i=1}^{n-1}\mathbf{J}_i^V\cdot\left[\frac{\nabla\mu_i}{T}+\frac{\bar{V}_i}{\bar{V}_n}\sum_{j=1}^{n-1}\frac{\rho_j}{\rho_n}\frac{\nabla\mu_j}{T}\right] , \tag{8}$$

and after rearranging dummy indices the phenomenological equations can be written as

$$\mathbf{J}_i^V=-\sum_{k=1}^{n-1}\frac{\nabla\mu_k}{T}\left[\sum_{j=1}^{n-1}\left[\delta_{jk}+\frac{\bar{V}_j\rho_k}{\bar{V}_n\rho_n}\right]L_{ij}\right] \quad (i=1,2,\ldots,n-1) . \tag{9}$$

In laboratory experiments diffusion is studied by measuring concentration gradients, $\nabla\rho_i$. Because of the identity

$$\sum_{i=1}^{n}\bar{V}_i\rho_i=1 \tag{10}$$

there are $n-1$ independent mole densities: $\rho_1,\rho_2,\ldots,\rho_{n-1}$. We may then use (10) to write the phenomenological equations (9) in terms of $n-1$ concentration gradient driving forces $\nabla\rho$:

$$\mathbf{J}_i^V=-\sum_{l=1}^{n-1}\frac{\nabla\rho_l}{T}\left\{\sum_{k=1}^{n-1}\frac{\partial\mu_k}{\partial\rho_l}\left[\sum_{j=1}^{n-1}\left[\delta_{jk}+\frac{\bar{V}_j\rho_k}{\bar{V}_n\rho_n}\right]L_{ij}\right]\right\} \quad (i=1,2,\ldots,n-1) , \tag{11}$$

where the partial derivatives $\partial\mu_i/\partial\rho_j$ are evaluated holding $\rho_{k\neq j}$ fixed.

The chemical or mutual-diffusion coefficients are defined by

$$\mathbf{J}_i^V=-\sum_{k=1}^{n-1}D_{ik}^V\nabla\rho_k \quad (i=1,2,\ldots,n-1) . \tag{12}$$

Here, D_{ik}^V is an element of an $(n-1)\times(n-1)$ matrix of chemical diffusivities, and the superscript V refers to the volume-fixed reference frame. These chemical diffusivities may be expressed in terms of the phenomenological coefficients L_{ij} by equating (11) and (12).

In summary, the $(n-1)\times(n-1)$ chemical diffusivity matrix D_{ik}^V assumes that there are n^2 phenomenological constants connecting each of n "forces" to each of the n diffusion fluxes J_i^V. The number of constants is reduced from n^2 to $(n-1)^2$ by application of the continuity equation and the Gibbs-Duhem equations. Onsager's reciprocal relationship postulates that the phenomenological coefficients l_{ij} and L_{ij} are symmetric (i.e., $l_{ij}=l_{ji}$, etc.). We do not make use of that symmetry here, but we note that symmetry of l and L does not carry over to symmetry in D.

In contrast to this general approach, the empirical models postulate n independent mobilities and specific microscopic dynamics to satisfy the continuity equation.

In Cooper's model the molar flux of species i is divided into a diffusion term and an advection term [8,12]:

$$\mathbf{J}_i^V=-\rho_i\frac{D_i}{RT}\nabla\mu_i+\rho_i\mathbf{u}^r \quad (i=1,2,\ldots,n) , \tag{13}$$

where D_i is the self-diffusivity of species i, D_i/RT defines its mobility, and R is the gas constant. Here, $\mathbf{u}^r$ is the relaxation velocity that is assumed common to all species. The value of $\mathbf{u}^r$ is determined by the continuity equation (4),

$$\mathbf{u}^r=\sum_{i=1}^{n}\bar{V}_i\rho_i\frac{D_i}{RT}\nabla\mu_i . \tag{14}$$

Substituting (14) into (13) and replacing $\nabla\mu_i$ with $\nabla\rho_i$ as the driving force we may write Cooper's model as

$$\mathbf{J}_i^V=-\rho_i\sum_{k=1}^{n-1}\nabla\rho_k\left[\sum_{j=1}^{n-1}\left[\delta_{ij}\frac{D_i}{RT}-\rho_j\bar{V}_j\frac{D_j}{RT}+\rho_j\bar{V}_n\frac{D_n}{RT}\right]\times\frac{\partial\mu_j}{\partial\rho_k}\right] \quad (i=1,2,\ldots,n-1) . \tag{15}$$

The molar flux of component i is the common force model is also written as the sum of a diffusion term and an advection term, but the latter is characterized by a common force $\mathbf{F}$ [9,10],

$$\mathbf{J}_i^V=-\rho_i\frac{D_i}{RT}\nabla\mu_i+\rho_i\bar{V}_i\frac{D_i}{RT}\mathbf{F} \quad (i=1,2,\ldots,n) . \tag{16}$$

The constraint (4) requires that

$$\mathbf{F}=\sum_{i=1}^{n}\rho_i\phi_i\nabla\mu_i , \tag{17a}$$

where the factor ϕ is a molar volume-weighted average mobility of the system given by [10]

$$\phi_i=\frac{\bar{V}_i D_i}{\sum_{j=1}^{n}\bar{V}_j^2\rho_j D_j} . \tag{17b}$$

In terms of concentration gradients the common force model is

$$\mathbf{J}_i^V=-\rho_i\frac{D_i}{RT}\sum_{k=1}^{n-1}\nabla\rho_k\left[\sum_{j=1}^{n-1}(\delta_{ij}-\bar{V}_i\rho_j\phi_j+\bar{V}_i\rho_j\phi_n)\frac{\partial\mu_j}{\partial\rho_k}\right] \quad (i=1,2,\ldots,n-1) . \tag{18}$$

Combining (12) and (15) yields a general expression for the relations between chemical and self-diffusion coefficients, along with other thermodynamic quantities, implied by Cooper's model. Similarly, combining (12) and (18) gives the relations implied by the common force model. In the present study we are only interested in binary systems. The explicit expressions for $n=2$ are

$$D_{11}^{Vd}=\rho_1\bar{V}_2(\rho_2 D_1+\rho_1 D_2)\frac{1}{RT}\frac{\partial\mu_1}{\partial\rho_1} \tag{19}$$

for Darken's model (the $n=2$ case of Cooper's model, and denoted by the superscript d), and

$$D_{11}^{Vc}=\frac{\rho_1\bar{V}_2 D_1 D_2}{\bar{V}_1^2\rho_1 D_1+\bar{V}_2^2\rho_2 D_2}\frac{1}{RT}\frac{\partial\mu_1}{\partial\rho_1} , \tag{20}$$

for the common force model (superscript c).

To proceed further it is necessary to express the chemical potential gradients in terms of concentration gradients. This requires additional constitutive models specific to the chemical systems being investigated. The rare gas system we study here is nearly ideal. In the particular case of ideality we have $\mu_i=\mu_i^0+RT\ln x_i$, with $x_i=\rho_i/\rho$ the molar fraction of i. By assuming ideality Eqs. (19) and (20) reduce to

$$D_{11}^{Vd}=x_2 D_1+x_1 D_2 \tag{21}$$

and

$$D_{11}^{Vc}=\frac{D_1 D_2}{\rho(\bar{V}_1^2\rho_1 D_1+\bar{V}_2^2\rho_2 D_2)} , \tag{22}$$

respectively. If additionally the partial molar volumes of species 1 and 2 are equal, i.e., $\bar{V}_1=\bar{V}_2=1/\rho$, the common force model takes the simple form

$$D_{11}^{Vc}=\frac{D_1 D_2}{x_1 D_1+x_2 D_2} . \tag{23}$$

B. Microscopic equations for the diffusion coefficients

In molecular dynamics simulations the flux of species i is defined relative to the center-of-mass velocity $\mathbf{u}^m=\sum_{i=1}^{n}c_i\mathbf{u}_i$ as [16]

$$\mathbf{J}_i^m=\rho_m c_i(\mathbf{u}_i-\mathbf{u}^m) , \tag{24}$$

where c_i is the mass fraction of component i and ρ_m the total mass density, $\rho_m=\sum_{i=1}^{n}m_i\rho_i$, with m_i the molar mass of species i. Summing (24) over species gives trivially

$$\sum_{i=1}^{n}\mathbf{J}_i^m=0 . \tag{25}$$

The center-of-mass reference frame is defined by the condition $\mathbf{u}^m=\mathbf{0}$, which is the case in an NVE ensemble (particle number N, volume V, energy E) molecular dynamics simulation. In this ensemble the momentum of the system is conserved and may, without loss of generality, be set to zero. The species velocity $\mathbf{u}_i$ is given by the individual particle velocities:

$$\mathbf{u}_i=\frac{1}{N_i}\sum_{\nu=1}^{N_i}\mathbf{v}_\nu , \tag{26}$$

where N_i is the number of particles of species i and $\mathbf{v}_\nu$ is the velocity of particle ν of species i. The phenomenological equations equivalent to (12), but in the center-of-mass reference frame, are

$$\mathbf{J}_i^m=-\rho_m\sum_{k=1}^{n-1}D_{ik}^m\nabla c_k \quad (i=1,2,\ldots,n-1) . \tag{27}$$

In order to relate these center-of-mass chemical diffusivities D_{ij}^m to those defined in the volume-fixed reference frame, D_{ij}^V, we need to relate the fluxes $\mathbf{J}_i^m$ and $\mathbf{J}_i^V$, and define the derivatives of mass fractions with respect to molar density. The two fluxes are related through the velocities $\mathbf{u}_1,\mathbf{u}_2,\ldots,\mathbf{u}_n$, which are equal in the two reference frames. For example, the volumetric reference velocity $\mathbf{u}^V$ defined in (3b) can be expressed in terms of $\mathbf{J}_i^m$, giving

$$\mathbf{J}_i^V=\sum_{k=1}^{n-1}\mathbf{J}_k^m\left[\frac{\delta_{ik}}{m_i}+\rho_i\left[\frac{\bar{V}_n}{m_n}-\frac{\bar{V}_k}{m_k}\right]\right] . \tag{28}$$

The derivatives $\partial c_i/\partial\rho_j$ are obtained by expressing c_i and ρ_j in terms of the constants m_i and $\bar{V}_i$ (see Ref. [5] for details),

$$\frac{\partial c_i}{\partial\rho_j}=\frac{1}{\rho_m}\left[m_i\delta_{ij}+c_i\left[m_n\frac{\bar{V}_j}{\bar{V}_n}-m_j\right]\right] \quad (i,j=1,2,\ldots,n-1) , \tag{29}$$

where $\partial c_i/\partial\rho_j$ is differentiated at fixed $\rho_{k\neq j}$. Equations (12), (27), (28), and (29) specify D_{ij}^V in terms of D_{ij}^m and vice versa. In general these diffusivities are not equal. However, in the binary case the single chemical diffusivity D_{11} is independent of reference frame: $D_{11}^m=D_{11}^V$. Moreover, since the self-diffusivities D_i are also independent of reference frame, in binary systems the equations for Darken's model [e.g., (21)] and for the common force model [e.g., (23)] are independent of reference frame.

The Green-Kubo formula for the chemical diffusion coefficient is obtained by combining the phenomenological equation (27) with the equation of conservation of mass, and solving these equations in the frequency domain and in reciprocal space. Details are given in Ref. [16]. We consider a binary system of N_1 atoms of type 1

and N_2 atoms of type 2. The single chemical diffusivity in this system is given by the one-sided Fourier transform of a collective velocity correlation function:

$$D_{11}(\omega)=\frac{Q}{3Nx_1x_2}\int_0^{t_{\max}\to\infty}\langle \mathbf{j}(t+\tau)\cdot\mathbf{j}(\tau)\rangle\exp(i\omega t)dt \ , \tag{30a}$$

where $N=N_1+N_2$ is the total number of particles. Here $\mathbf{j}(t)$ is a collective quantity of particle velocities,

$$\mathbf{j}(t)=x_2\sum_{\nu=1}^{N_1}\mathbf{v}_\nu-x_1\sum_{\nu=1}^{N_2}\mathbf{v}_\nu \ , \tag{30b}$$

and Q is a thermodynamic factor defined by

$$Q=[1+x_1x_2\rho(\Gamma_{11}+\Gamma_{22}-2\Gamma_{12})]^{-1} \ , \tag{30c}$$

with

$$\Gamma_{ij}=4\pi\int_0^\infty r^2[g_{ij}(r)-1]dr \ . \tag{30d}$$

In the last equation $g_{ij}(r)$ is the radial distribution function for the pair of species ij. Equations (30c) and (30d) give necessary recipes for computing the thermodynamic factor Q in a molecular dynamics simulation. It may be shown [27] that Q is related to the compositional derivative of chemical potential by $Q=(x_1/RT)(\partial\mu_1/\partial x_1)$. For ideal solutions it follows immediately that $Q=1$ and from (30c) that $\Gamma_{11}+\Gamma_{12}-2\Gamma_{22}=0$.

The self-diffusion coefficients are given by the similar but simpler expression

$$D_j(\omega)=\tfrac{1}{3}\int_0^{t_{\max}\to\infty}c_j(t)\exp(i\omega t)dt \ , \tag{31a}$$

where $c_j(t)$ is the average over all particles of type j of the velocity autocorrelation function:

$$c_j(t)=\frac{1}{N_j}\sum_{\nu=1}^{N_j}\langle \mathbf{v}_\nu(t+\tau)\cdot\mathbf{v}_\nu(\tau)\rangle \ . \tag{31b}$$

The velocity correlation functions in Eqs. (30a) and (31b), $\langle \mathbf{v}_\nu(t+\tau)\cdot\mathbf{v}_\gamma(\tau)\rangle$, may be averaged over different time origins τ. Typically 10^4–10^5 time origins are used in our simulations and the angular bracket $\langle\ \rangle$ denotes such an ensemble average.

The diffusion coefficients given by (30) and (31) are frequency dependent. For comparison with laboratory diffusion experiments only the results in the low frequency limit $\omega\to 0$ are relevant. However, since the upper limit of integration $t_{\max}$ in Eqs. (30a) and (31a) is of necessity finite, frequencies lower than $2\pi/t_{\max}$ are not well constrained. The numerical results at $\omega=0$ are valid only if the system has no modes with characteristic time scales longer than $t_{\max}$. Diffusivities at high frequencies ($\omega\gg 2\pi/t_{\max}$) may be well constrained when the integrals (30a) and (31a) are truncated, even if diffusivities at lower frequencies are not.

There are two important differences between the formulas for the chemical diffusion coefficient (30) and self-diffusion coefficient (31). First, the thermodynamic Q factor in Eq. (30a) gives the chemical diffusion coefficient a thermodynamic dependency that is lacking in the self-diffusion coefficient. However, for a thermodynamically ideal mixture $Q=1$ and the thermodynamic dependency of D_{11} is removed. Second, the correlation function for D_i is a single-particle property, which can be averaged over N_i atoms of the same type, whereas the correlation function appearing in D_{11} is a collective quantity that permits no such averaging. This makes a profound difference in the statistical precision with which these terms may be determined in a numerical simulation.

If we expand the expression for D_{11} (30a) and group separately the velocity autocorrelations and cross correlations, D_{11} may be written as

$$D_{11}(\omega)=x_2D_1(\omega)+x_1D_2(\omega)+x_1x_2\left[\frac{f_{11}(\omega)}{x_1^2}+\frac{f_{22}(\omega)}{x_2^2}-2\frac{f_{12}(\omega)}{x_1x_2}\right] . \tag{32}$$

The f functions [28] are the Fourier transforms of the velocity cross-correlation functions given explicitly by

$$f_{11}(\omega)=\frac{1}{3N}\sum_{\nu=1}^{N_1}\sum_{\gamma\neq\nu}^{N_1}\int_0^{t_{\max}\to 0}\langle \mathbf{v}_\nu(t+\tau)\cdot\mathbf{v}_\gamma(\tau)\rangle\times\exp(i\omega t)dt \ , \tag{33a}$$

$$f_{22}(\omega)=\frac{1}{3N}\sum_{\nu=1}^{N_2}\sum_{\gamma\neq\nu}^{N_2}\int_0^{t_{\max}\to 0}\langle \mathbf{v}_\nu(t+\tau)\cdot\mathbf{v}_\gamma(\tau)\rangle\times\exp(i\omega t)dt \ , \tag{33b}$$

$$f_{12}(\omega)=\frac{1}{3N}\sum_{\nu=1}^{N_1}\sum_{\gamma=1}^{N_2}\int_0^{t_{\max}\to 0}\langle \mathbf{v}_\nu(t+\tau)\cdot\mathbf{v}_\gamma(\tau)\rangle\times\exp(i\omega t)dt \ . \tag{33c}$$

Comparing (32) with (21) it follows immediately that we must satisfy

$$\frac{f_{11}(\omega)}{x_1^2}+\frac{f_{22}(\omega)}{x_2^2}-2\frac{f_{12}(\omega)}{x_1x_2}=0 \tag{34}$$

in order to obtain the generalization of Darken's model,

$$D_{11}(\omega)=x_2D_1(\omega)+x_1D_2(\omega) \ . \tag{35}$$

Similarly, a comparison of (32) with (23) indicates that

$$\frac{f_{11}(\omega)}{x_1^2}+\frac{f_{22}(\omega)}{x_2^2}-2\frac{f_{12}(\omega)}{x_1x_2}=-\frac{[D_1(\omega)-D_2(\omega)]^2}{x_1D_1(\omega)+x_2D_2(\omega)}<0 \tag{36}$$

is necessary to generalize the common force model,

$$D_{11}(\omega)=\frac{D_1(\omega)D_2(\omega)}{x_1D_1(\omega)+x_2D_2(\omega)} \ . \tag{37}$$

The denominator on the right-hand side of (36) and (37) is

the average self-diffusivity of the system. It can be seen from (36) that the common force model implies a negative net contribution of cross correlations to the chemical diffusivity. Hence D_{11} given by the common force model is less than or equal to that given by Darken's model. The difference between the two models becomes trivial when the two self-diffusivities are similar.

In this section we indicated how microscopic variables in molecular dynamics experiments may be used to deduce self-diffusivities [D_1 and D_2, Eq. (31)] and chemical diffusivities [D_{11}, Eq. (30)]. Specific relationships amongst the cross correlations that are required to give Darken's and the common force model were presented [Eqs. (34) and (36)]. This gives the theoretical background that allows us to test whether a given binary system may be well represented by a particular empirical diffusion model. The generalization of these results to several ($n>2$) components is straightforward but lengthy. In Sec. V we apply these results to our Ar-Kr simulation results, described below.

III. SIMULATION REMARKS

In this study we conducted simulations in the *NVE* ensemble. The atoms interact via a Lennard-Jones (L-J) potential,

$$\psi_{ij}=4\epsilon_{ij}\left[\left[\frac{\sigma_{ij}}{r}\right]^{12}-\left[\frac{\sigma_{ij}}{r}\right]^{6}\right]. \tag{38}$$

The potential parameters governing interactions between unlike atoms are given by the Lorentz-Berthelot mixing rules,

$$\sigma_{ij}=(\sigma_{11}+\sigma_{22})/2 \tag{39a}$$

and

$$\epsilon_{12}=(\epsilon_{11}\epsilon_{22})^{1/2}. \tag{39b}$$

The L-J parameters for the model argon and krypton atoms are given in Table I. We truncated the potential at a cutoff radius, discussed below, and made appropriate corrections to the potential energy and pressure using the method described in Ref. [20].

Atoms are confined in a cubic box and initially placed at fcc sites. Their positions and velocities are advanced according to the leapfrog algorithm [29]. Periodic boundary conditions are employed. The system is allowed to equilibrate for 2×10^4 to 5×10^4 time steps until the thermodynamic quantities T and P stabilize to their equilibrium values, which we judge by an absence of systematic drift. Velocity correlation functions and radial distribution functions are calculated from the data stored during the simulation, but not during the equilibration period.

TABLE I. Lennard-Jones potential parameters (from Ref. [20]).

Molecule	m (g/mol)	ϵ/k_B (K)	σ (Å)
Ar	39.95	120	3.405
Kr	83.80	167	3.633

Before doing any simulations of binary systems we did a few trial runs on pure Ar to test our programs against other published results. The first trial run we made is for a system of 108 Ar atoms at a density of $0.85/\sigma^3$, with a cutoff radius of 2.5σ. With an energy of $(-4.617\,68\pm0.000\,04)\epsilon$ we obtained an equilibrium temperature of $(0.88\pm0.05)\epsilon/k_B$, and pressure of $(1.21\pm0.30)\epsilon/\sigma^3$ using data collected over 20 000 time steps following equilibration. These P and T values are consistent with the equation of state of argon given by Verlet [30]. The self-diffusivity of Ar calculated from the mean squared displacement (i.e., the Einstein relation) is 1.59×10^{-5} cm^2/s.

In the second trial, we did a simulation of the same system at the same thermodynamic state but using Ewald's method [31] to evaluate the r^{-6} part of the potential and forces exactly. Since this program and the one used in the first test were coded independently, comparing the results of this second run with those of the first provides a double check. The convergence parameter for the Ewald sum was chosen as $\eta=L/5$. For this run at $E=(-4.617\,69\pm0.000\,04)\epsilon$ we obtained $T=(0.88\pm0.04)\epsilon/k_B$ and $P=(1.20\pm0.31)\epsilon/\sigma^3$ after equilibration. The results are in good agreement with those of the previous trial. Although there is no apparent truncation effect on the internal energy, temperature, or pressure, the self-diffusivity of Ar for this run is 1.86×10^{-5} cm^2/s, which suggests this dynamical property may be sensitive to the truncation of the long-range potential. To make certain that the diffusivity was computed correctly we carried out a third trial run with 864 Ar atoms, density $0.81/\sigma^3$, for comparison with Rahman's diffusivity simulation result [32]. This simulation used an $L/2$ cutoff radius of 10.2σ instead of Ewald's method. At $T=(0.79\pm0.01)\epsilon/k_B$, we calculated the diffusion constant of Ar to be 2.52×10^5 cm^2/s. This number is slightly greater than Rahman's value (2.43×10^{-5} cm^2/s), but is within the range of statistical errors. Our value is also consistent with the measured diffusivity of Ar at $T=0.75\epsilon/k_B$, 2.43×10^{-5} cm^2/s [32].

The good energy conservation, the internal consistency of our trial runs, and the generally good agreement between our results and prior studies demonstrate that the simulations are correctly implemented in our programs.

IV. SIMULATION RESULTS FOR BINARY Ar-Kr MIXTURES

Four binary system simulations were performed in this study: three 512-particle simulations at different compositions and one 1728-particle simulation at equimolar composition (see Table II). All the simulations were run at the same nominal pressure and temperature. A time step of approximately 0.01 ps was used, which gave energy conservation to two parts in 10^5 during the entire simulations which consisted of $O(10^6)$ time steps. The potential interactions were truncated at half of the simulation cell edge length ($L/2$). After equilibration we

TABLE II. Simulation runs and the corresponding equilibrium states.

Run	N_{Ar}/N_{Kr}	Time steps	L (Å)	ρ_m (g/cm^3)	T (K)[a]	P (MPa)[a]
1	256/256	10^6	30.56	1.84	121.7±2.7	0.82±5.9
2	384/128	9×10^5	30.52	1.52	121.3±2.7	0.82±5.8
3	128/384	5×10^5	30.66	2.15	121.1±2.8	0.92±5.9
4	864/864	4.62×10^5	45.85	1.84	120.4±1.4	0.52±3.2

[a]Errors are estimated from rms fluctuations.

stored the coordinate and velocity of each atom in the system at every fifth time step. Diffusivities were computed later from these stored simulation results.

The time origins τ we average over are offset by about 0.05 ps (5 time steps). In a study by Schoen and Hoheisel [19] they found that the characteristic decay time of their correlation functions was 0.3 ps. By averaging over time origins separated from one another by less than this time scale, we are effectively including redundant information that reduces the effectiveness of the averaging. However, the total number of averages we take is so large, $O(10^4-10^5)$, that this effect does not materially effect our results. To verify this we tried a computation averaged over 2×10^4 origins, each spaced 0.3 ps (30 time steps) apart. The resulting mean squared displacement functions were indistinguishable from those obtained with a 0.05 ps spacing. Subsequent calculations are based on a 0.05 ps spacing between time origins τ.

A. Thermodynamic properties

We compute the radial distribution functions $g_{ij}(r)$ from the ensemble average of histograms of interparticle separation. The results for run 1 are shown in Figs. 1(a)–1(c) to half of the length of the cubic box ($L/2\approx15$ Å). It can be seen that these functions approach the ideal gas limit, $1-\delta_{ij}/N_i$, for large r [16].

The factor $1/N_i$ is insignificant in the thermodynamic limit $N\to\infty$. However, that factor may result in a finite contribution to Γ_{ij} even in the thermodynamic limit since the Γ_{ij} are integrals of the radial distribution functions over the entire volume of the system. Thus a nontrivial correction is needed. Integrating the $g_{ij}(r)$ functions in Figs. 1(a)–1(c) and dividing the results by the factor $1-\delta_{ij}/N_i$, we obtain the Γ_{ij} for run 1. Figure 1(d) shows some combinations of the Γ_{ij} as a function of the upper limit in the integration of (30d), r_{max}, nondimensionalized by the number density of the system. It is apparent that the Γ_{ij} are fast oscillating functions of r_{max}, and that the fluctuations of Γ_{ij} become smaller as r_{max} increases. According to (30c) the combination $\Gamma_{11}+\Gamma_{22}-2\Gamma_{12}$, when evaluated at $r_{max}\to\infty$, should be zero for an ideal system. It is apparent in Fig. 1(d) that this function tends to a value in the range (0,0.2), which indicates a slight departure from ideality.

It is difficult to assess the errors in extrapolating these functions to $r_{max}\to\infty$, but an uncertainty of 0.2 in $\Gamma_{11}+\Gamma_{22}-2\Gamma_{12}$ lets us take $Q=1$ with an uncertainty of about 10%. Accordingly, in what follows we assume ideality.

The other functions of Γ_{ij} shown in Fig. 1(d) are related to the partial molar volumes through (see Ref. [27])

$$\bar{V}_1=Q[1+\rho_2(\Gamma_{22}-\Gamma_{12})]/\rho \tag{40a}$$

and

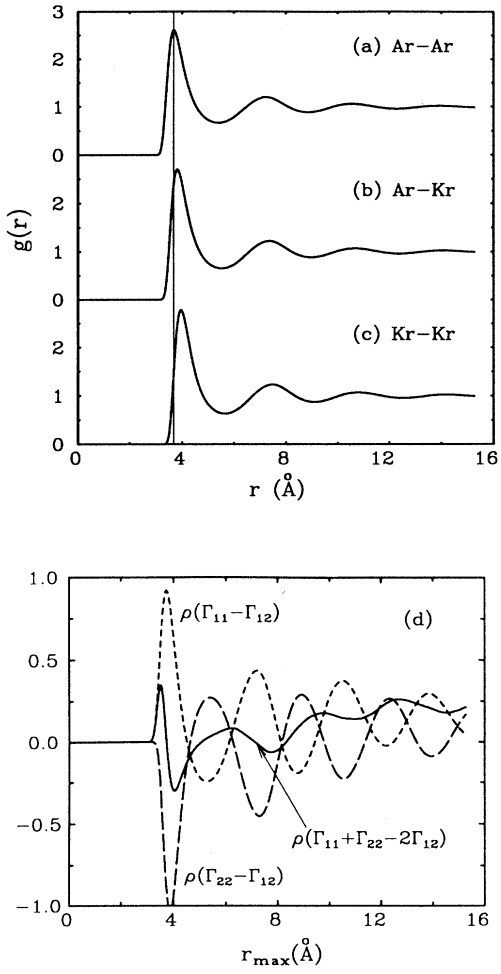

FIG. 1. Radial distribution functions for 512-particle equimolar system (run 1), averaged over 2×10^5 configurations. (a) $g_{11}(r)$, (b) $g_{12}(r)$, and (c) $g_{22}(r)$. The vertical thin line is shown to facilitate comparison. (d) Combinations of their spatial integrals Γ_{ij} plotted against the upper limit of integration and nondimensionalized by the number density ρ.

$$\bar{V}_2 = Q[1+\rho_1(\Gamma_{11}-\Gamma_{12})]/\rho \ . \tag{40b}$$

Since the combinations $\Gamma_{22}-\Gamma_{12}$ and $\Gamma_{11}-\Gamma_{12}$ tend to zero as $r_{\max}\to\infty$, the partial molar volumes of Ar and Kr are approximately equal in this simulation. We therefore use Eq. (23) instead of the more complicated Eq. (22) for the common force model. The uncertainty associated with this assumption probably amounts to $<10\%$. Since the ratio $\bar{V}_1/\bar{V}_2$ is independent of Q, the equal molar volume approximation and the ideality approximation are independent.

B. Accuracy, precision, and comparison with earlier results

In Fig. 2(a) we present the velocity correlation functions for Ar, Kr, and the collective Ar-Kr mode at short times. The simulation consisted of 512 total particles in equal proportions (Table II, run 1). The real parts of the frequency-dependent diffusivities, obtained from the Fourier transform of these correlation functions by Eqs. (30a) and (31a), are shown in Fig. 2(b). We obtained these results using an upper time limit of integration $t_{\max}=20$ ps, and averaging the results over approximately 2×10^5 time origins τ. Note that the frequency axis is logarithmic to emphasize the behavior at comparatively low frequencies. The results at $\omega=0$ are indicated by the symbols on the vertical axis. The qualitative features seen in Fig. 2(b) are consistent with those computed by Rahman for pure Ar [32]. The diffusivities have a maximum at intermediate frequencies, followed by a plateau at lower frequencies. The frequency-dependent diffusivities appear insensitive to frequency at the lowest frequencies we can resolve. Unless low frequency modes exist that are undetected in our study, the results presented for this run in Table III ought to be comparable to laboratory time scale experiments (assuming the validity of the potential model, etc.).

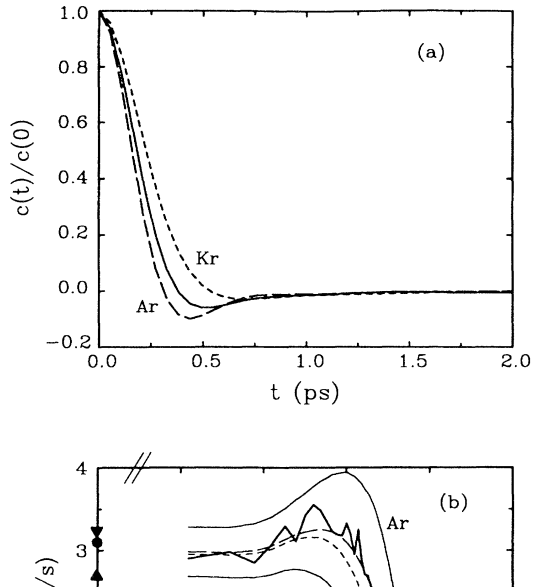

FIG. 2. (a) Normalized 20-ps-long velocity correlation function for run 1. The solid line is for D_{11}, the long dashed line for $D_{\rm Ar}$, and the short dashed line for $D_{\rm Kr}$. (b) The corresponding frequency spectra on a logarithmic scale. Thin solid lines are self-diffusivities of Ar and Kr, and the thick solid line is D_{11}. The long and short dashed lines are the chemical diffusivities predicted by Darken's model and the common force model, respectively.

To make a quantitative assessment of the probable error in the zero-frequency diffusivity caused by truncation of $t_{\max}$ it is necessary to introduce model assumptions for the long-time tail of the velocity correlation functions. The truncated diffusivity $\tilde{D}(\omega)$ and the "exact" diffusivity $D(\omega)$ are related by

$$\begin{aligned}\tilde{D}(\omega) &= \int_0^{t_{\max}} dt\, e^{i\omega t} c(t) \\ &= D(\omega) - \int_{t_{\max}}^{\infty} dt\, e^{i\omega t} c(t) \ .\end{aligned} \tag{41}$$

If we assume that the long-time tail of the velocity correlation function is given by the hydrodynamic result [16,23]

$$\lim_{t\to\infty} c(t) \to c_0 t^{-3/2} \tag{42}$$

the correction term in (41) may be bounded as follows:

$$\begin{aligned}\left| \int_{t_{\max}}^{\infty} dt\, e^{i\omega t} c(t) \right| &\le c_0 \int_{t_{\max}}^{\infty} dt \left| e^{i\omega t} t^{-3/2} \right| \\ &\le c_0 \int_{t_{\max}}^{\infty} dt \left| t^{-3/2} \right| \\ &= \frac{2c_0}{\sqrt{t_{\max}}} \ .\end{aligned} \tag{43}$$

Therefore, if our truncation is within the hydrodynamic regime (42) the effect of truncation is to introduce an error proportional to $t_{\max}^{-1/2}$. The constant of proportionality c_0 must be determined separately for each diffusivity mode in each simulation from the measured long-time behavior of the appropriate correlation functions. Unfortunately, we cannot resolve the long-time tail of $c(t)$ in any of our simulations. Within our ability to measure it the coefficient c_0 in (43) is zero, and so the effect of the truncation of $t_{\max}$ should be negligible within our statistical errors.

Fluctuations in the diffusivity spectra can be used to estimate their precision. It is evident in Fig. 2(b) that the self-diffusivities of Ar and Kr have essentially no uncertainty in comparison with the much larger uncertainty for the chemical diffusivity D_{11}. As noted earlier, this is

TABLE III. Diffusion coefficients in 10^{-5} cm^2/s for the equimolar systems.

	$N=512$				$N=1728$	
	VCF[a]		MSD[b]		VCF	MSD
t_{max}:	20 ps	80 ps	20 ps	80 ps	20 ps	20 ps
D_{Ar}	3.26	3.25	3.27	3.26	3.37	3.34
D_{11}	3.12	2.91	3.19	3.04	3.68	3.30
D_{Kr}	2.71	2.70	2.70	2.70	2.78	2.74

[a]From velocity correlation functions at zero frequency.
[b]From mean squared displacement at t_{max}.

because the self-diffusivities may be averaged over all particles of a given type but no such averaging is possible for the chemical diffusivity. Increasing the number of particles improves the precision of the self-diffusivities but not the chemical diffusivity. Both diffusivities are averaged over time origins τ. For a given t_{max}, the number of origins τ may be increased only by increasing the total run time of the simulation. The computation shown in Fig. 2(b) consisted of 10^6 time steps, and cost ≈ 17 Cray Y-MP CPU hours. Even with such a long run the fluctuations in chemical diffusivity suggest a precision of order 10% at low frequencies.

There is a trade-off between accuracy and precision. For a run with a fixed number of time steps decreasing t_{max} allows the integrand to be averaged over a larger number of time origins, which in turn gives chemical diffusivities of higher precision. The cost for this reduction in t_{max} is an increase in the lowest resolved frequency $\omega_{min}=2\pi/t_{max}$. The connection between behaviors at $\omega=0$ and ω_{min} becomes more problematic, and the accuracy of the result (from the point of view of laboratory time scale experiments) suffers. In Fig. 3 we show the real part of the frequency-dependent diffusivities computed from the same data used to construct Fig. 2(b), but increasing t_{max} from 20 to 80 ps. The number of time origins is reduced by a factor of 1200 [i.e., 1200=(80 ps−20 ps)/(0.05 ps/record)]. Our lowest nonzero frequency is now extended from 0.2 to 0.1 ps^{-1}, but the precision estimated from the magnitude of the fluctuations is greatly reduced. No new low frequency behavior was discovered by extending the frequency range. The diffusivities computed with $t_{max}=80$ ps are also given in Table III.

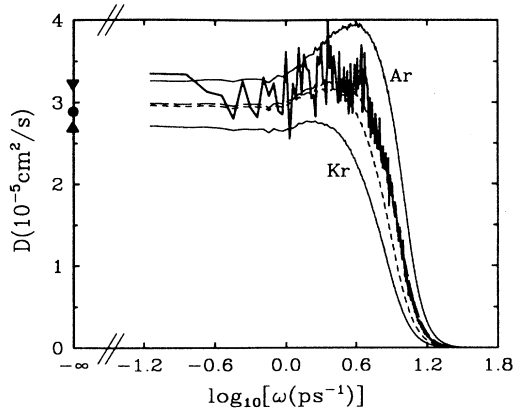

FIG. 3. As Fig. 2(b), but from 80-ps-long velocity correlation functions.

We also compute diffusivities using mean squared displacements. We define the time-dependent self-diffusivity of component j to be [26]

$$D_j(t)=\frac{\langle |r(t)-r(0)|^2\rangle}{6t} . \tag{44}$$

When evaluated in the limit of infinite time this gives the Einstein result

$$D_j^{\text{Einstein}}=\lim_{t\to\infty} D_j(t) , \tag{45}$$

which is formally equivalent to the Green-Kubo expression (31a) when $t_{max}=\infty$ [16]. Here r is the coordinate of a particle of type j, and the average $\langle\ \rangle$ is over all particles of this type. The mutual-diffusion coefficient is obtained in an analogous manner using the collective displacement [cf. Eq. (30b)]

$$r_{12}(t)=x_2\sum_{\nu=1}^{N_1} r_\nu(t)-x_1\sum_{\nu=1}^{N_2} r_\nu(t) . \tag{46}$$

The time-dependent self-diffusivity (44) may be written in terms of the velocity autocorrelation function $c(t)$ by [16]

$$D_j(t)=\int_0^t ds\left[1-\frac{s}{t}\right]c(s) . \tag{47a}$$

We may express $c(t)$ in terms of the frequency-dependent self-diffusivity through the inverse transform of (31a). Combining these expressions gives

$$D_j(t)=\frac{1}{2\pi}\int_0^\infty d\omega\, D_j(\omega)\int_0^t ds\left[1-\frac{s}{t}\right]e^{i\omega s}$$
$$=\frac{1}{2\pi t}\int_0^\infty d\omega\, D_j(\omega)\left[\frac{1+i\omega t-e^{i\omega t}}{\omega^2}\right] ; \tag{47b}$$

a similar transformation relates the time- and frequency-dependent mutual-diffusion coefficients.

In Fig. 4 we show the mean squared displacements for

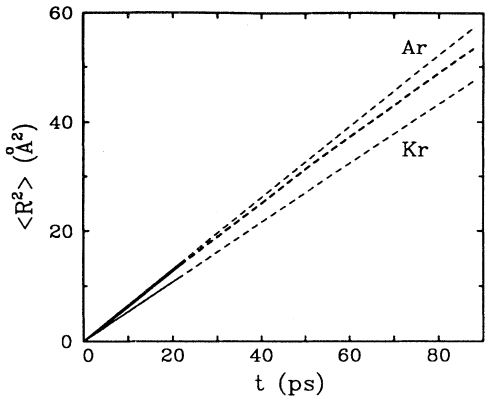

FIG. 4. Mean squared displacements as a function of time for run 1. The solid lines are for $t_{max}=20$ ps and the dashed lines for $t_{max}=80$ ps. The thick lines are for D_{11} and the thin lines for D_{Ar} and D_{Kr}.

run 1 to $t_{max}=20$ ps, and the resulting time-dependent diffusivities are shown in Fig. 5. The strong time dependence of the diffusivities at short time is related to their strong frequency dependence at high frequencies. At long times the mean squared displacements appear linear, but a slight curvature remains in Fig. 4 that translates into a residual slope in the time-dependent diffusivities shown in Fig. 5. This is particularly evident in the time-dependent mutual-diffusion coefficient. The self-diffusivities obtained from mean squared displacements are in excellent agreement with the velocity correlation results (Table III). The mutual diffusivities are in somewhat poorer agreement, probably because of the greater scatter evident in Figs. 2(b) and 3. We estimate the statistical errors for this run to be about 10% for chemical diffusivity and 0.5% for self-diffusivities.

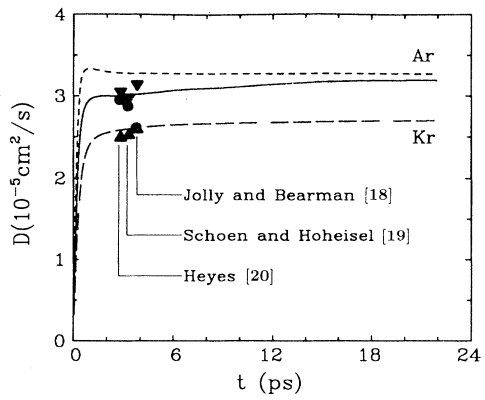

FIG. 5. Time-dependent diffusivities from the Einstein relations for $t_{max}=20$ ps of run 1 (D_{11}, solid line; D_{Ar}, short dashed line; D_{Kr}, long dashed line), with the results of Refs. [18–20]: D_{Ar} (downward triangles), D_{Kr} (upward triangles), and D_{11} (circles).

In Fig. 5 we also compared our time-dependent diffusivities with those of previous workers. Heyes and co-workers [33,20] reported a correlation integral time t_{max} of ≈ 2.5 ps, Schoen and Hoheisel [19] ≈ 3.0 ps, and

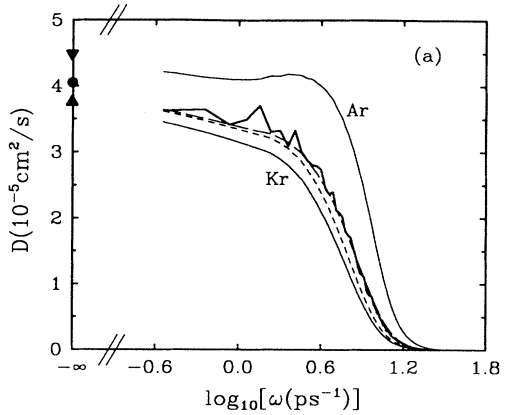

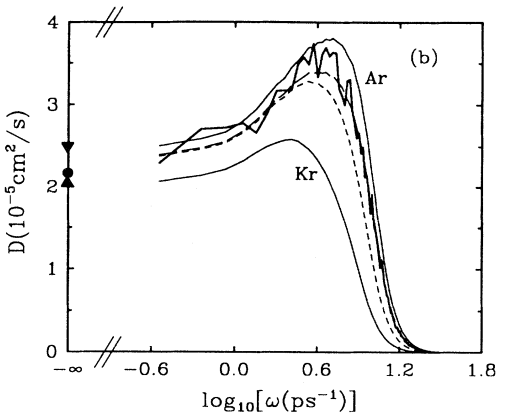

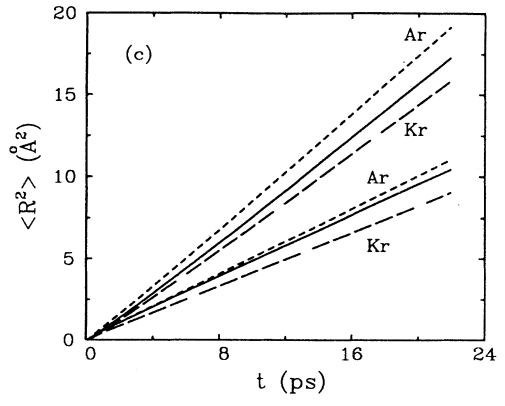

FIG. 6. Spectra of 20-ps-long velocity correlation functions for $Ar_{0.75}Kr_{0.25}$ (a) and $Ar_{0.25}Kr_{0.75}$ (b). See Fig. 2(b) caption. (c) Mean squared displacements with $t_{max}=20$ ps. The top three lines are for $Ar_{0.75}Kr_{0.25}$, and the bottom three lines for $Ar_{0.25}Kr_{0.75}$: solid lines, D_{11}, short dashed lines, D_{Ar}, and long dashed lines, D_{Kr}.

TABLE IV. Diffusion coefficients in 10^{-5} cm^2/s for the nonequimolar systems.

	$Ar_{0.75}Kr_{0.25}$				$Ar_{0.25}Kr_{0.75}$	
	VCF		MSD		VCF	MSD
t_{max}:	20 ps	80 ps	20 ps	80 ps	20 ps	20 ps
D_{Ar}	4.51	5.15	4.36	4.71	2.51	2.52
D_{11}	4.07	4.64	3.94	4.31	2.19	2.38
D_{Kr}	3.77	4.41	3.61	3.97	2.06	2.06

Jolly and Bearman [18] ≈ 3.5 ps. Our diffusivity coefficients at $t_{max} \approx 20$ ps are somewhat larger than those found in the previous studies, and by inference the disagreement would be greater if our correlation times were even longer. The agreement is improved if our time-dependent diffusion coefficients, evaluated at the integral time reported by other workers, are compared to the diffusion coefficients they reported. What differences remain may be attributed to statistical uncertainties and differences in implementation. For example, we use 512 atoms whereas Heyes and Schoen and Hoheisel use 256 and Jolly and Bearman use 864.

C. Dependence on composition

To examine the dependence of the diffusivities on composition we carried out simulations at compositions $Ar_{0.75}Kr_{0.25}$ (run 2) and $Ar_{0.25}Kr_{0.75}$ (run 3). The volume and energy of these systems are slightly different, and different from run 1 described above, to give the same simulation pressure and temperature (Table II). The real parts of the frequency-dependent diffusivities for these runs are shown in Figs. 6(a) and 6(b), respectively. These were computed using $t_{max}=20$ ps, but averaged over only 1.8×10^5 and 8×10^4 time origins for reasons of economy. The diffusivity coefficients for these runs are given in Table IV.

A comparison of these frequency-dependent diffusivities with those of run 1 shown in Fig. 2(b) shows a surprisingly strong composition dependence. The diffusivity values at low frequency decrease in the order $Ar_{0.75}Kr_{0.25} > Ar_{0.5}K_{0.5} > Ar_{0.25}Kr_{0.75}$. Increasing the abundance of Ar, by itself a faster diffusing species, increases the self-diffusivity of Kr and also increases the chemical diffusivity. In contrast to the $Ar_{0.5}Kr_{0.5}$ results [Figs. 2(b) and 3], the frequency-dependent diffusivities in $Ar_{0.75}Kr_{0.25}$ and $Ar_{0.25}Kr_{0.75}$ do not exhibit a low frequency plateau. It is therefore apparent that some low frequency modes of the system ($\omega \leq 2\pi/t_{max}$) are not adequately resolved with $t_{max}=20$ ps. The static $\omega=0$ values indicated must therefore be regarded with some skepticism. The existence of low frequency modes is also evident in plots of mean squared displacement [Fig. 6(c)] which are clearly nonlinear in the time interval [0,20 ps].

To explore the low frequency behavior evident in $Ar_{0.75}Kr_{0.25}$ we computed the frequency-dependent diffusivities with $t_{max}=80$ ps. This result, shown in Fig. 7(a), is noisier than Fig. 6(a) because the results are averaged over a smaller number of time origins. Nevertheless, it is apparent that the strong frequency dependence continues to frequencies lower than $2\pi/80$ ps^{-1}. This is also seen in the curvature of the mean squared displacements shown in Fig.7(b).

In Fig. 8 we compare our $t_{max}=20$ ps velocity correlation diffusivities for all three compositions with the results of Heyes [20]. In general our results agree well with Heyes, but our measured diffusivities increase with increasing Ar fraction more than his. This is consistent with the dependence of diffusivity on correlation integral time, as illustrated in Fig. 5, and on the frequency-

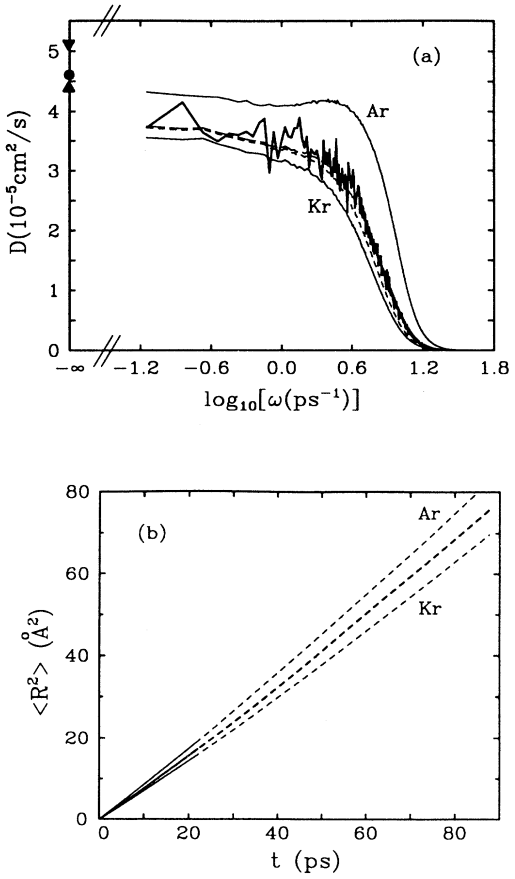

FIG. 7. (a) As Fig. 2(b), but from 80-ps-long velocity correlation functions and for $Ar_{0.75}Kr_{0.25}$. (b) As for Fig. 5, but for $Ar_{0.75}Kr_{0.25}$.

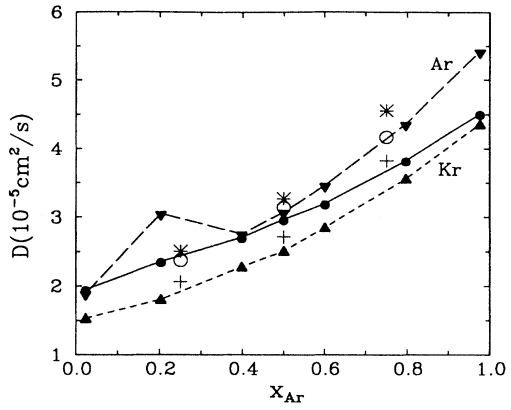

FIG. 8. Compositional dependence of the diffusivities in Ar-Kr binary mixtures. Solid symbols with lines are results of Heyes [20]: D_{Ar} (downward triangles), D_{Kr} (circles), and D_{11}(upward triangles). Our results (Tables III and IV) are represented by stars (D_{Ar}), plus signs (D_{Kr}), and empty circles (D_{11}).

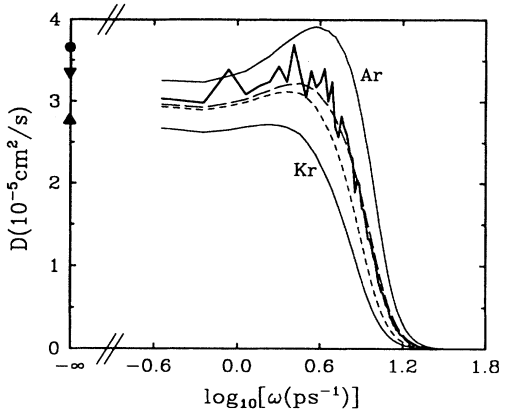

FIG. 9. As Fig. 2(b), but for 1728-particle system (run 4).

dependent behaviors seen in Figs. 2(b), 6(a), and 6(b). The frequency dependence of Kr rich $Ar_{0.25}Kr_{0.75}$ [Fig. 6(b)] suggests that increasing t_{max} will decrease the diffusivities at that composition; whereas the frequency dependence of Ar rich $Ar_{0.75}Kr_{0.25}$ [Fig. 6(a)] suggests that increasing t_{max} will increase the diffusivities. Thus by increasing the correlation time from Heyes's 2.5 ps to our 20 ps value, we tend to increase the diffusivities of Ar rich compositions relative to Ar poor compositions. The trend may be accidental—the relevant diffusivity is $t_{max}\rightarrow\infty$, and this may be either greater than or less than the results presented here. The point we emphasize here is that these results are sensitive to the correlation integral time, and the discrepancy between our result and Heyes's may be explained by our different values of t_{max} and by the specific frequency dependences seen in Figs. 2(b), 6(a), and 6(b).

D. Effect of simulation size

A fundamental question regarding molecular dynamics simulations is whether the properties of a small and periodic sample are necessarily representative of the properties of a macroscopic aperiodic system [29]. Our run 4 (Table II) has the equimolar composition used in run 1, but uses 1728 particles in a correspondingly larger periodic simulation cell. For reasons of computational efficiency, our r^{-6} potential term is truncated at $L/2$; thus in effect we are changing both particle size and the truncation distance. Our results on pure Ar using Ewald's method suggest that increasing the truncation distance (from $L/2$ to ∞) may raise the diffusivity by 10%. Here we have increased the cutoff distance by a factor of $\sqrt[3]{1728/512}=\frac{3}{2}$. We do not expect this to have a dramatic effect on the diffusivities, but the possibility must be acknowledged.

The frequency-dependent diffusivities for run 4, computed with $t_{max}=20$ ps, are shown in Fig. 9. They are almost identical to those in Fig. 2(b), but there are two subtle differences. First, the fluctuations seen in the chemical diffusivity in Fig. 9 are much larger than seen in Fig. 2(b), sometimes breaking the bracket formed by the Ar and Kr self-diffusivities. This is probably due to the smaller number of time origins used ($\approx 8\times10^4$ vs 2×10^5). Second, a slight slope in the frequency-dependent diffusivities is evident in Fig. 9, suggesting that a low frequency mode may be present that was undetected in Fig. 2(b). Because of this slope, the diffusivities computed for this run are systematically larger than those computed for run 1 (Table III).

Reports of the N dependence of diffusion coefficients in the literature are rather controversial (e.g., [34] and references therein). It is commonly believed that transport coefficients are nearly independent of N, but both increases and decreases in the self-diffusivity of Ar have been reported on increasing the number of particles [34]. Additional work on this problem is necessary. This may prove to be particularly interesting in view of the possibility that N dependence and t_{max} dependence maybe coupled through the low frequency mode suggested by Fig. 9.

V. EMPIRICAL DIFFUSION MODELS

The above discussions are relevant to assessing how accurate and precise numerical simulations are in relation to laboratory data (values in the limit $N\rightarrow\infty, t_{max}\rightarrow\infty$, and $\omega\rightarrow0$). Of course this is also sensitive to the interatomic force model which we take here as given. Despite the difficulties described above, there are aspects of these simulations that are useful for elucidating relationships between the microscopic dynamics and macroscopic transport coefficients that hold true regardless of the faithfulness of the model to any specific "real" system. It is in this spirit we test our simulations against the empirical models to begin a systematic study of the applicability of those relationships.

The self-diffusivities of Ar and Kr shown in Figs. 2(b), 3, 6(a), 6(b), 7(a), and 9 may be used to compute the frequency-dependent Darken model chemical diffusivity [Eq. (35)] and the common force model chemical diffusivity [Eq. (37)]. Long dashed lines in Figs. 2(b), 4, 6(a), 6(b), 7(a), and 9 represent the Darken model calculation, and short dashed lines in those figures are for the common force model. In each of these figures Darken's model is consistent with the velocity correlation function determination of the chemical diffusivity over the entire frequency range that is resolved. At low frequencies the chemical diffusivities predicted by Darken's model and by the common force model tend to converge, and our velocity correlation results have larger uncertainty. Therefore at frequencies lower than about 5 ps^{-1} we cannot discriminate between the two models.

We showed in Eq. (34) that the term $f_{11}/x_1^2+f_{22}/x_2^2-2f_{12}/x_1x_2$ must be zero if Darken's model is exactly correct. In Fig. 10(a) we show this term evaluated in the time domain, and in Fig. 10(b) in the frequency domain, from data collected in run 1 where $x_1=x_2=0.5$. It is evident in Fig. 10(b) that the condition necessary for Darken's model to work is well satisfied over the entire resolved frequency range. Similar results for runs 2 and 3 are shown in Fig. 11.

The sum $f_{11}/x_1^2+f_{22}/x_2^2-2f_{12}/x_1x_2$ may deviate from zero in either direction [6]. Small positive deviations have been found for highly dissymmetric L-J model mixtures [35] and some nonelectrolyte solutions [6]. These positive departures are inconsistent with both the empirical models we consider. Negative deviations have been found for some other nonelectrolyte solutions [6] and for molten salts [36]. As demonstrated in Eq. (36) the sum is negative when the common force model works. The negativity of this term for molten salts allows the possibility that the common force model would apply to that Coulombic system. The good agreement of the common force model for silicate systems [10], which are also characterized by strong Coulombic interactions, suggests a connection between the dominance of Coulombic forces and applicability of the common force model.

The individual velocity cross-correlation terms f_{11},

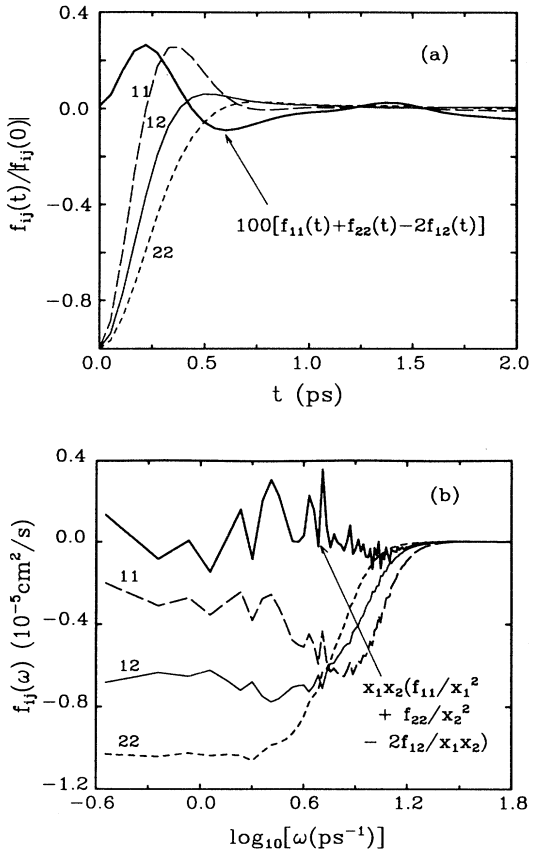

FIG. 10. Normalized velocity cross-correlation functions (a) and their spectra (b) for run 1. In both diagrams, the long dashed lines, the short dashed lines, and the thin solid lines are the cross correlations due to Ar-Ar interactions, Kr-Kr interactions, and Ar-Kr interactions, respectively. The thick solid lines are the combination of them as indicated in the figures [see Eq. (32)].

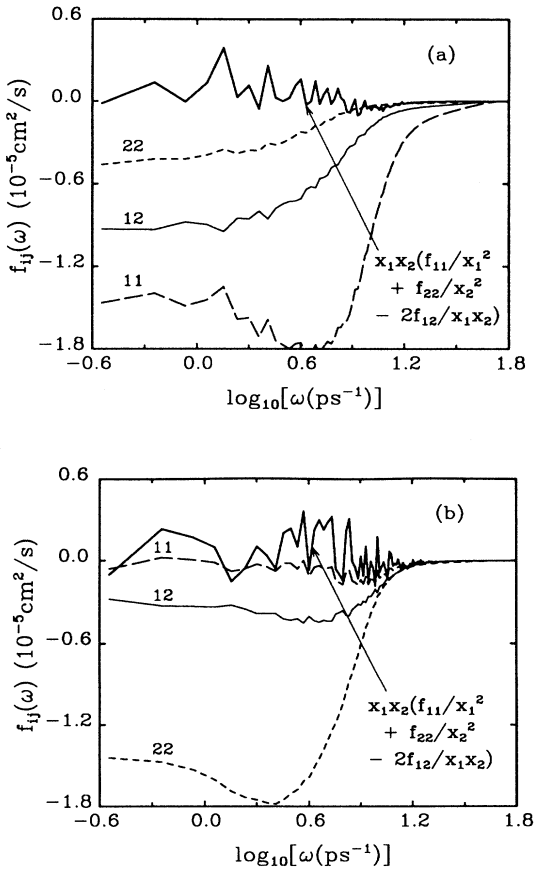

FIG. 11. As Fig. 10(b), but for $Ar_{0.75}Kr_{0.25}$ (a) and $Ar_{0.25}Kr_{0.75}$ (b).

f_{22}, and f_{12} are substantial and negative at low frequencies, Figs. 10(b), 11(a), and 11(b). The assumption that cross correlations are zero ([16], p. 289), which may be used to derive Darken's model, is clearly contradicted by these calculations (see also [28]).

The negativity of these velocity cross correlations may be explained qualitatively as follows. The negativity of f_{12} results from the requirement of the conservation of momentum. Conservation of momentum requires that

$$m_1\sum_{\nu}^{N_1}\mathbf{v}_\nu+m_2\sum_{\gamma}^{N_2}\mathbf{v}_\gamma=0 \tag{48}$$

at all times. Squaring this result gives

$$2m_1m_2\sum_{\nu}^{N_1}\sum_{\gamma}^{N_2}\langle\mathbf{v}_\beta\cdot\mathbf{v}_\gamma\rangle = -m_1^2\left|\sum_{\nu}^{N_1}\mathbf{v}_\nu\right|^2-m_2^2\left|\sum_{\gamma}^{N_2}\mathbf{v}_\gamma\right|^2<0\ . \tag{49}$$

Since at $t=0$ the magnitude of the correlation is larger than at other times, (49) is expected to dominate f_{12} (33c), and so this term is likely negative.

To interpret f_{11} and f_{22} we image a system where the particle velocities within a species i are randomly distributed, and the average particle velocity of the species $N_i^{-1}\sum_{\nu=1}^{N_i}\mathbf{v}_\nu$ is zero. In our Ar-Kr models this assumption is valid. Consequently the sum of the cross correlations within a single species, $\mathbf{v}_\nu\cdot\sum_{\gamma\neq\nu}^{N_i}\mathbf{v}_\gamma$, must be negative even though individual cross correlations $\mathbf{v}_\nu\cdot\mathbf{v}_{\gamma\neq\nu}$ could be positive, negative, or zero. Again, since the correlations at $t=0$ are expected to dominate we would predict $f_{11}<0$ (33a) and $f_{22}<0$ (33b).

It is interesting to note that in Ar-dominated $Ar_{0.75}Kr_{0.25}$ [Fig. 11(a)] the largest cross-correlation term is f_{11}, whereas in Kr-dominated $Ar_{0.25}Kr_{0.75}$ [Fig. 11(b)] the largest term is f_{22}. At the intermediate composition $Ar_{0.5}Kr_{0.5}$ [Fig. 10(b)] the f_{11} term dominates at high frequency, but f_{22} dominates at low frequency. This is qualitatively consistent with the expectation that Ar will contribute preferentially to higher frequency modes because of its lower mass.

VI. CONCLUSIONS

Two empirical diffusion models that relate chemical diffusivities to self-diffusivities and thermodynamic properties are described at the level of the phenomenological equations and using the microscopic statistical theory of liquids. Assumptions that yield Darken's model and the common force model are discussed. The model relations are compared with molecular dynamics simulation results for four binary Ar-Kr mixtures. Self- and chemical diffusivities of the simulated systems are calculated from the Fourier spectrum of velocity correlation functions and from mean squared displacements. We have made special efforts to obtain reliable diffusivities by calculating the velocity correlation functions and mean squared displacements over comparatively long correlation times (20–80 ps).

The computed chemical diffusivities are consistent with Darken's model in the entire frequency range realized in the simulations. At high frequencies where the frequency-dependent diffusivities have small fluctuations the common force model is not compatible with the simulation results within statistical errors. At low frequencies the spectra have large fluctuations and the two models cannot be discriminated with confidence. The difference in the models results from different assumptions made for the cross-correlation functions. Calculations of the cross correlations for the simulated systems indicate that the overall contribution of cross correlations to the chemical diffusivity is indeed approximately zero, as assumed in Darken's model. However, individual cross correlations are significant and negative.

ACKNOWLEDGMENTS

We are grateful to Yan Liang and Frank M. Richter for many stimulating discussions and for allowing us to cite their unpublished results. This work was supported by NSF Grant No. EAR-9304263 and the Alcoa Foundation (G.H.M.), and by NSF Grant No. EAR-9316390 (F. M. Richter). The computations were supported by the National Center for Supercomputing Applications, University of Illinois at Urbana-Champaign, and by the Pittsburgh Supercomputing Center.

[1] B. E. Watson and D. R. Baker, in *Physical Chemistry of Magmas,* edited by I. Kushiro and L. Perchuk (Springer-Verlag, Berlin, 1991), p. 120.
[2] Y. Liang, F. M. Richter, and B. E. Watson, Nature **369**, 390 (1994).
[3] Y. Zhang, J. Geophys. Res. **98**, 11 901 (1993).
[4] C. E. Lesher, J. Geophys. Res. **99**, 9585 (1994).
[5] S. R. D. Groot and P. Mazur, *Non-Equilibrium Thermodynamics* (Dover, New York, 1984).
[6] D. W. McCall and D. C. Douglass, J. Phys. Chem. **71**, 987 (1967).
[7] L. S. Darken, Trans. AIME **175**, 184 (1948).
[8] A. R. Cooper, Phys. Chem. Glasses **6**, 55 (1965).
[9] A. C. Lasaga, Geochim. Cosmochim. Acta **43**, 455 (1979).
[10] Y. Liang, Ph.D. thesis, University of Chicago, 1994.
[11] R. J. Bearman, J. Phys. Chem. **65**, 1961 (1961).
[12] F. M. Richter, Geochim. Cosmochim. Acta **57**, 2019 (1993).
[13] R. Mills, R. Malhorta, L. A. Woolf, and D. G. Miller, J. Phys. Chem. **98**, 5565 (1994).
[14] D. Levesque, L. Verlet, and J. Krkijarvi, Phys. Rev. A **7**, 1680 (1973).
[15] G. Ciccotti, D. Frenkel, and I. R. McDonald, *Simulation of Liquids and Solids—Molecular Dynamics and Monte Carlo Methods in Statistical Mechanics* (North-Holland, Amsterdam, 1987).
[16] J. P. Hansen and I. R. McDonald, *Theory of Simple Liquids* 2nd ed. (Academic, London, 1986).

[17] R. Zwanzig, Annu. Rev. Phys. Chem. **16**, 67 (1965).
[18] D. L. Jolly and R. J. Bearman, Mol. Phys. **41**, 137 (1980).
[19] M. Schoen and C. Hoheisel, Mol. Phys. **52**, 33 (1984).
[20] D. M. Heyes, J. Chem. Phys. **96**, 2217 (1992).
[21] D. J. Pine, D. A. Weitz, P. M. Chaikin, and E. Herbolzheimer, Phys. Rev. Lett. **60**, 1134 (1988).
[22] D. A. Weitz, D. J. Pine, P. N. Pusey, and R. J. A. Tough, Phys. Rev. Lett. **63**, 1747 (1989).
[23] J. X. Zhu *et al.*, Phys. Rev. Lett. **68**, 2559 (1992).
[24] M. H. Kao, A. G. Yodh, and D. J. Pine, Phys. Rev. Lett. **70**, 242 (1993).
[25] A. J. C. Ladd, Phys. Rev. Lett. **70**, 1339 (1993).
[26] I. Zúñiga and P. Español, Phys. Rev. Lett. **71**, 3665 (1993).
[27] J. G. Kirkwood and F. Buff, J. Chem. Phys. **19**, 774 (1951).
[28] J. Trullàs and J. A. Padró, Phys. Rev. E **50**, 1162 (1994).
[29] M. P. Allen and D. J. Tildesley, *The Computer Simulation of Liquids* (Oxford University Press, London, 1987).
[30] L. Verlet, Phys. Rev. **159**, 98 (1967).
[31] N. Karasawa and W. A. Goddard III, J. Phys. Chem. **93**, 7320 (1989).
[32] A. Rahman, Phys. Rev. **136**, A405 (1964).
[33] P. J. Gardner, D. M. Heyes, and S. R. Preston, Mol. Phys. **73**, 141 (1991).
[34] J. J. Erpenbeck, Phys. Rev. A **35**, 218 (1987).
[35] M. Schoen and C. Hoheisel, Mol. Phys. **52**, 1029 (1984).
[36] J. P. Hansen and I. R. McDonald, Phys. Rev. A **11**, 2111 (1975).